

**STRUCTURAL AND MAGNETIC PROPERTIES OF
DISORDERED CRYSTALLINE $\text{Fe}_{50}\text{Mn}_{25+x}\text{Sn}_{25-x}$ ALLOYS
WITH $x = -1.25, 0.0, 2.5, 5.0, 7.5$**

***PROPIEDADES ESTRUCTURALES Y MAGNÉTICAS DE
ALEACIONES CRISTALINAS DESORDENADAS
 $\text{Fe}_{50}\text{Mn}_{25+x}\text{Sn}_{25-x}$ CON $x = -1.25, 0.0, 2.5, 5.0, 7.5$***

**Wilber Pachín¹, Víctor A. Peña¹, Misael León², Chachi Rojas¹,
José J. Medina¹, Carlos V. Landauro¹, Justiniano Quispe¹, Jorge
Agüero¹, Edson C. Passamani³, Elisa Baggio-Saitovitch⁴**

¹ Facultad de Ciencias Físicas, Universidad Nacional Mayor de San Marcos, Lima, Perú.

² Facultad de Ciencias, Universidad Nacional de Ingeniería, Lima, Perú.

³ Departamento de Física, Universidade Federal do Espírito Santo, Vitória, ES, Brazil.

⁴ Centro Brasileiro de Pesquisas Físicas, Rio de Janeiro, Brazil.

(Recibido: 05/2020. Aceptado: 08/2020)

Abstract

Disordered crystalline $\text{Fe}_{50}\text{Mn}_{25+x}\text{Sn}_{25-x}$ alloys, with $x = -1.25, 0.0, 2.5, 5.0, 7.5$ (close to the full-Heusler alloys), were arc-melted in a high purity argon atmosphere and the molten pellets were individually sealed in quartz tubes also under argon atmosphere. Subsequently, they were annealed at 1173 K for 4 days, being finally quenched in a bath with cold water. Structural and magnetic properties have systematically been studied using X-ray diffraction, ^{57}Fe , and ^{119}Sn Mössbauer spectroscopies, and magnetization measurements recorded at room temperature. Rietveld refinement of the X-ray diffraction patterns of the annealed samples with $x = -1.25$ and 0 has revealed the presence of two hexagonal crystallographic phases: (i) a chemically disordered solid solution identified as $\varepsilon-(\text{Fe}/\text{Mn})_3\text{Sn}$ (majority fraction) and (ii) the $\varepsilon-\text{Fe}_5\text{Sn}_3$ intermetallic compound (minority fraction). For samples

with $x = 2.5, 5.0,$ and $7.5,$ the Rietveld analysis has only indicated the presence of a chemically disordered solid solution identified as $\varepsilon-(\text{Fe/Mn})_3(\text{Sn/Fe/Mn})$. Although compositions of the $\text{Fe}_{50}\text{Mn}_{25+x}\text{Sn}_{25-x}$ alloys are close to that of full-Heusler alloys, none of them has the expected $L2_1$ structure. The average crystallite sizes, estimated from the Williamson-Hall method, are in the range of 256-62 nm. The average sizes has gradually decreased as the x -content is increased. Mössbauer results have shown localized-type magnetism from Fe non-equivalent sites, and itinerant-like magnetism on ^{119}Sn -probes. Magnetic hysteresis loops, recorded at 300 K for a maximum field of 2200 Oe, have indicated that the remanent and coercive fields have systematically decreased as the x -parameter has increased. Coercive fields are in the range for soft magnets (1-20 Oe).

Keywords: ^{57}Fe Mössbauer spectroscopy, ^{119}Sn Mössbauer spectroscopy, disordered solid solutions, transferred magnetic hyperfine fields, Heusler alloys.

Resumen

Aleaciones cristalinas desordenadas $\text{Fe}_{50}\text{Mn}_{25+x}\text{Sn}_{25-x}$, con $x = -1.25, 0.0, 2.5, 5.0, 7.5,$ cercanas a las composiciones de Heusler-211, fueron preparadas por fusión en atmósfera inerte, subsecuentemente, sometidas a recocido térmico durante 4 días a 1173 K y, finalmente, enfriadas en agua helada. Todas las aleaciones han sido sistemáticamente analizadas mediante difracción de rayos X, espectroscopias Mössbauer de ^{57}Fe y ^{119}Sn , y medidas de magnetización a temperatura ambiente. Los análisis Rietveld de los difractogramas de las muestras con $x = -1.25$ y 0.0 muestran la presencia de dos fases cristalográficas hexagonales: (i) la solución sólida químicamente desordenada $\varepsilon-(\text{Fe/Mn})_3\text{Sn}$ (mayoritaria), y (ii) el intermetálico $\varepsilon-\text{Fe}_5\text{Sn}_3$ (minoritaria); mientras que, las aleaciones con $x = 2.5, 5.0$ y $7.5,$ presentan solo la solución sólida desordenada, $\varepsilon-(\text{Fe/Mn})_3(\text{Sn/Fe/Mn})$. Si bien, las composiciones de las aleaciones $\text{Fe}_{50}\text{Mn}_{25+x}\text{Sn}_{25-x}$ son cercanas a las de Heusler-211, ninguna tiene la

estructura cúbica $L2_1$ característica de estas. Los tamaños medios de los cristalitas, calculados por el método de Williamson-Hall, están dentro del rango 62-256 nm y disminuyen cuando x aumenta. Los resultados Mössbauer de todas las aleaciones muestran la característica de magnetismo localizado a través de la distribución de campos magnéticos hiperfinos en los sitios de Fe, y de magnetismo itinerante a través de los campos transferidos desde los átomos de Fe en los núcleos de ^{119}Sn . Los campos coercitivos y remanentes, obtenidos por medidas de magnetización bajo campo magnético aplicado entre -2200 y +2200 Oe, disminuyen cuando x aumenta. Los valores de los campos coercitivos están en el rango de los magnetos blandos (1-20 Oe).

Palabras clave: Espectroscopia Mössbauer del ^{57}Fe , espectroscopia Mössbauer del ^{119}Sn , soluciones sólidas desordenadas, campos hiperfinos magnéticos transferidos, aleaciones de Heusler.

Introduction

Many research groups in the entire world are currently working on the development of new alloys with soft magnetic properties for technological applications in spintronic, biomedicine, magnetic sensors, and energy. The full Heusler alloys or compositions close to them, in particular, have systematically attracted the interest of the scientific community due to their great variety of magneto-structural effects, such as: high magnetocaloric, ferromagnetically shaped memory, semi-metallicity, exchange bias, magneto-resistive, among others [1–12].

In general, Heusler alloys of the X_2YZ type (full-Heusler alloy) consist of two transition metal atoms, X and Y, with the number of electrons d : $n_d > 5$ and $n_d \leq 5$, respectively, and one non-metal atom, Z, with the number of d electrons $n_d = 0$ or 10, and hybridizations of the sp -type. At room temperature (RT), the X_2YZ Heusler alloys have a centered body cubic structure, $L2_1$ -type ($Fm\bar{3}m$), with the Y and Z atoms interconnected between two

tetrahedral lattices, occupying the centers of each cube of X atoms (austenitic phase).

In the case of Heusler ferromagnetic alloys with $Y = \text{Mn}$ [13–16], the Mn atoms may usually play the role of electron spin-polarizer. Otherwise, the X atom is responsible for changing the lattice parameter of the $L2_1$ phase, as well as providing the localized electrons ($3d$) and conduction electrons ($4s$), responsible for the localized and itinerant magnetism, respectively. Z atoms act as non-magnetic spacers regulating the exchange interaction, constituting a source of sp electrons that participate in the magnetic interaction between Mn atoms (indirect exchange coupling). In the case of Mn-based Heusler alloys, their magnetic properties depend primarily on the distance between manganese atoms (Mn-Mn), which in turn, depends on the lattice parameter of the $L2_1$ phase.

For instance, studies on Fe_2MnSn Heusler alloys with compositions close to the full Heusler have recently been reported [17–19]. For example, V. K. Jain et al. [17] have studied the nanocrystallization – by mechanical grinding (high energy ball-milling)– of the Fe_2MnSn Heusler alloy, previously prepared by melting a blend of elemental powders. It has combined experimental (analysis of X-ray diffraction and DC magnetization measurements) and also theoretical (calculations of state density and band structure) approach to show that the initial molten sample has presented an $L2_1$ -type majority phase (full Heusler structure), with a lattice parameter equal to 6.246 \AA , co-existing with a tetragonal-like phase. However, the nanocrystallization process of the samples has shown a gradual reduction of the tetragonal phase, but there is a gap in the literature related to the investigation of order-disorder phases as well as magnetic properties of Fe_2MnSn alloys in different crystalline structures.

In the present work, we studied the micro-granular structure of the arc-melted and annealed $\text{Fe}_{50}\text{Mn}_{25+x}\text{Sn}_{25-x}$ alloys with $x = -1.25, 0.0, 2.5, 5.0, 7.5$ (close to the full-Heusler alloys). It has been shown that the $L2_1$ -type structure is not stabilized. However, due to rapid cooling (quenching), the formation of the $\varepsilon-(\text{Fe}/\text{Mn})_3\text{Sn}$ and

ε -(Fe/Mn)₃(Sn/Fe/Mn) phases are favored, both with hexagonal D0₁₉-type symmetry (space group: $P63/mmc$), where the Mn atoms randomly share the sites ($6h$) with Fe and Sn. Local (⁵⁷Fe and ¹¹⁹Sn Mössbauer spectroscopies) and bulk (X-ray diffraction and magnetization) measurements were employed to understand the structural and magnetic properties of these alloys.

1. Experimental procedure

1.1. Sample preparation

The Fe₅₀Mn_{25+x}Sn_{25-x} system, with x -1.25, 0.0, 2.5, 5.0, 7.5 (the minus sign “-” corresponds to a fraction of Mn that is subtracted from Heusler’s composition) was prepared using an arc-melting furnace under a controlled and high purity argon atmosphere. Five Fe-Mn-Sn alloys were prepared from mixtures of high purity elemental powders of Fe (99.5%), Mn(99.9%), and Sn(99.9%). In order to ensure homogeneity of the alloys, the melting process of each mixture was repeated, at least, five times, rotating the solidified sample inside the casting chamber. The mass of each prepared solid sample was approximately 2 g (the loss of mass after the melting process is less than 2%). Subsequently, each solid sample (previously sealed in a quartz tube, under argon atmosphere) was annealed at 1173 K for 4 days and quenched in iced-water (a mixture of water and ice). The sample preparation process followed a methodology previously developed in our group, which guarantees the reproducibility of sample properties.

1.2. X-ray diffraction

The structural properties of the annealed alloys were analyzed by X-ray diffraction technique using a Bruker-D8 Focus diffractometer, operated at 40 kV and 40 mA with Cu-K α radiation ($\lambda = 1.5406\text{\AA}$). The percentage of the phases for each alloy, as well as the microstructural parameters (lattice parameters, atomic

occupations, phase fraction), were obtained by Rietveld refinement using the Topas software (Bruker AXS) [14]. The crystallite sizes and their internal micro-tensions were separately calculated by the Williamson-Hall method.

1.3. Mössbauer spectroscopy

The local magnetic orders of the annealed $\text{Fe}_{50}\text{Mn}_{25+x}\text{Sn}_{25-x}$ alloys were systematically studied by ^{57}Fe and ^{119}Sn Mössbauer spectroscopies. The ^{57}Fe and ^{119}Sn isotopes act as local probes in the study of the localized magnetism from the d -electrons of the Fe atoms and the itinerant magnetism of the conduction s -electrons, respectively. Likewise, considering that the spin polarization process is a global-like effect, Fe and Mn atoms also contribute to the itinerant magnetism character measured in the Sn sites (^{119}Sn isotopes only probe the transferred magnetic hyperfine fields).

The Fe and Sn Mössbauer spectra were obtained for all samples at RT using a transmission Mössbauer spectrometer, with standard radioactive sources of $^{57}\text{Co}/\text{Rh}$ (25 mCi) and $^{119m}\text{Sn}/\text{CaSnO}_3$ (5 mCi), respectively. The Mössbauer parameters [isomer shift (δ), magnetic hyperfine field (B_{hf}), linewidth (Γ), and absorption area (A)] in both Fe and Sn sites were obtained using the NORMOS program. The δ -values are relative to radioactive sources.

1.4. Magnetization measurement

Magnetic hysteresis loops $[M(H)]$ were recorded at RT for all annealed $\text{Fe}_{50}\text{Mn}_{25+x}\text{Sn}_{25-x}$ alloys using a vibrant sample magnetometer (VSM) from the Faculty of Sciences of the National University of Engineering. This is a local manufacturing equipment, with automatic measurement control, characterized by a sensitivity of 10^{-4} , capable of measuring magnetic moments on the order of 10 emu, under a maximum magnetic field of 2300 Oe. Calibration was performed using a Ni (99.9 %) disc (38 mm diameter, 120 mm thick, and 30.7 mg mass).

2. Results and discussion

2.1. Rietveld analysis of the XRD patterns of the $\text{Fe}_{50}\text{Mn}_{25+x}\text{Sn}_{25-x}$ powder alloys with x: -1.25, 0.0, 2.5, 5.0, 7.5

X-ray diffraction (XRD) patterns of the annealed $\text{Fe}_{50}\text{Mn}_{23.75}\text{Sn}_{26.25}$, $\text{Fe}_{50}\text{Mn}_{25}\text{Sn}_{25}$, $\text{Fe}_{50}\text{Mn}_{27.5}\text{Sn}_{22.5}$, $\text{Fe}_{50}\text{Mn}_{30}\text{Sn}_{20}$, and $\text{Fe}_{50}\text{Mn}_{32.5}\text{Sn}_{17.5}$ alloys are respectively shown in Figures 1 (a), (b), (c), (d), and (e). The Bragg peaks of the crystallographic phases, identified by Rietveld refinement, are also indicated in the XRD patterns.

Table 1 shows the structural parameters [lattice constant, average crystallite size $\langle D \rangle$, internal strain ($\langle \varepsilon^2 \rangle^{1/2}$), atomic occupancy (Ocp), and phase fraction (X_{ph})] obtained for each alloy from the Rietveld refinement and the Williamson-Hall method. The quality of Rietveld refinements is quantified by the low values of chi-squared (χ^2) [$\chi^2 = (R_{wp}/R_{exp})^2$, where R_{wp} and R_{exp} are weighted profile R-factor and expected R-factor factors, respectively]. The different occupations of the shared sites reflect the atomic disorder in each alloy.

The XRD patterns of the $\text{Fe}_{50}\text{Mn}_{23.75}\text{Sn}_{26.25}$ and $\text{Fe}_{50}\text{Mn}_{25}\text{Sn}_{25}$ alloys were fitted using two hexagonal crystalline phases: (i) a crystalline solid solution identified as the ε -(Fe/Mn) $_3$ Sn (majority phase), and (ii) the ε -Fe $_5$ Sn $_3$ intermetallic compound (minority phase). The ε -(Fe/Mn) $_3$ Sn solid solution has a hexagonal structure D0_{19} (spatial group $P6_3/mmc$), where Fe and Mn atoms share $6h$ Wyckoff sites and Sn atoms are located at $2c$ site.

The ε -Fe $_5$ Sn $_3$ intermetallic is described by the $P6_3/mmc$ spatial group, where Fe atoms are placed in two $2a$ and $2d$ Wyckoff sites. Moreover, Sn atoms are located at the $2c$ site. Figures 2 (a) and (b) show the observed (black) and calculated (red curve) XRD patterns of the $\text{Fe}_{50}\text{Mn}_{23.75}\text{Sn}_{26.25}$ and $\text{Fe}_{50}\text{Mn}_{25}\text{Sn}_{25}$ alloys, respectively. Below each XRD pattern, the difference in the intensities between observed and calculated diffraction patterns is also plotted.

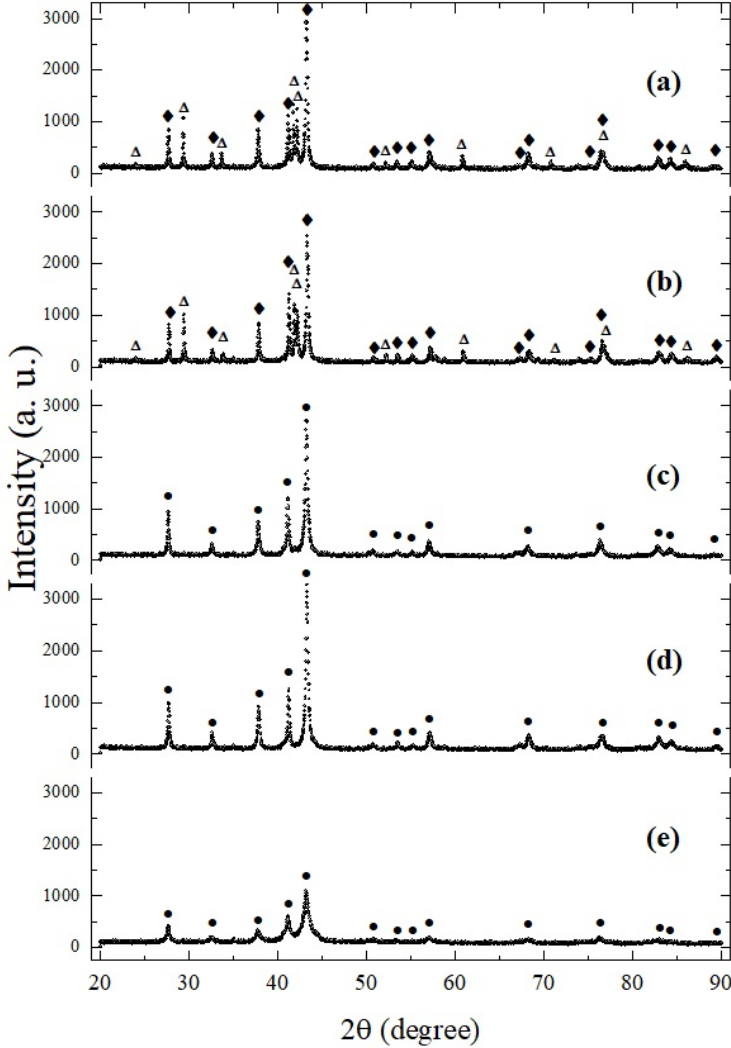


FIGURE 1. X-ray diffraction patterns of the $Fe_{50}Mn_{25+x}Sn_{25-x}$ alloys with: (a) $x = -1.25$, (b) $x = 0$, (c) $x = 2.5$, (d) $x = 5$, (e) $x = 7.5$. (◆) $[\varepsilon-(Fe/Mn)_3Sn]$, (Δ) $[\varepsilon-Fe_5Sn_3]$, and (●) $[\varepsilon-(Fe/Mn)_3(Sn/Fe/Mn)]$.

The first conclusion is that the $Fe_{50}Mn_{25}Sn_{25}$ alloy, despite X_2YZ composition, does not correspond to a full-Heusler alloy characterized by an $L2_1$ -type structure. The XRD patterns of the $Fe_{50}Mn_{27.5}Sn_{22.5}$, $Fe_{50}Mn_{30}Sn_{20}$, and $Fe_{50}Mn_{32.5}Sn_{17.5}$ alloys were fitted using a $\varepsilon-(Fe/Mn)_3(Sn/Fe/Mn)$ hexagonal phase. It

| x | Phase | Space group | Atom | W. S. | Ocp. | Lattice parameters | | | $\langle D \rangle$ (nm) | $\langle \varepsilon^2 \rangle^{1/2}$ | X _{ph} (%) | |
|--------|------------------------------------|----------------------|-------|-------|------|--------------------|---------|---------|-----------------------------|---------------------------------------|---------------------|--|
| | | | | | | a(Å) | b(Å) | c(Å) | | | | |
| - 1.25 | (Fe/Mn) ₃ Sn | P6 ₃ /mmc | Fe | 6h | 0.65 | | | | | | | |
| | | | Mn | 6h | 0.35 | 5.50(4) | 5.50(4) | 4.29(5) | 144(8) | 0.00124 | 93 | |
| | | | Sn | 2c | 0.96 | | | | | | | |
| | Fe ₅ Sn ₃ | P6 ₃ /mmc | Fe I | 2a | 1.0 | | | | | | | |
| | | | Fe II | 2d | 0.66 | 4.29(5) | 4.29(5) | 5.32(3) | 176(8) | 0.00062 | 7 | |
| | | | Sn | 2c | 0.96 | | | | | | | |
| 0.0 | (Fe/Mn) ₃ Sn | P6 ₃ /mmc | Fe | 6h | 0.62 | | | | | | | |
| | | | Mn | 6h | 0.38 | 5.50(3) | 5.50(3) | 4.38(4) | 160(8) | 0.00137 | 92 | |
| | | | Sn | 2c | 0.96 | | | | | | | |
| | Fe ₅ Sn ₃ | P6 ₃ /mmc | Fe I | 2a | 1.0 | | | | | | | |
| | | | Fe II | 2d | 0.5 | 4.29(4) | 4.29(4) | 5.31(5) | 180(8) | 0.00078 | 8 | |
| | | | Sn | 2c | 0.9 | | | | | | | |
| 2.5 | (Fe/Mn) ₃ (Sn/Fe/Mn) | P6 ₃ /mmc | Fe | 6h | 0.66 | | | | | | | |
| | | | Mn | 6h | 0.34 | | | | | | | |
| | | | Sn | 2c | 0.9 | 5.50(5) | 5.50(5) | 4.39(2) | 204(8) | 0.00213 | 100 | |
| | | | | Fe | 2c | 0.02 | | | | | | |
| | | | | Mn | 2c | 0.08 | | | | | | |
| | | | | Fe | 6h | 0.66 | | | | | | |
| 5.0 | (Fe/Mn) ₃ (Sn/Fe/Mn) | P6 ₃ /mmc | Mn | 6h | 0.34 | | | | | | | |
| | | | Sn | 2c | 0.80 | 5.50(4) | 5.50(4) | 4.38(3) | 256(8) | 0.00219 | 100 | |
| | | | Fe | 2c | 0.03 | | | | | | | |
| | | | | Mn | 2c | 0.17 | | | | | | |
| | | | | Fe | 6h | 0.65 | | | | | | |
| | | | | Mn | 6h | 0.35 | | | | | | |
| 7.5 | (Fe/Mn) ₃ (Sn/Fe/Mn) | P6 ₃ /mmc | Sn | 2c | 0.70 | | | | | | | |
| | | | Fe | 2c | 0.04 | 5.50(7) | 5.50(7) | 4.40(5) | 62(8) | 0.00420 | 100 | |
| | | | Mn | 2c | 0.26 | | | | | | | |

TABLE 1. Structural parameters obtained from Rietveld refinement of the XRD patterns of the annealed $Fe_{50}Mn_{25+x}Sn_{25-x}$ alloys with: (a) $x = -1.25$, (b) $x = 0$, (c) $x = 2;5$, (d) $x = 5$, (e) $x = 7.5$ [lattice constants (a, b, c), crystalline size $\langle D \rangle$, internal strain ($\langle \varepsilon^2 \rangle^{1/2}$), atomic occupancy (Ocp), and percentage of the phases (X_{ph})].

is described by $P6_3/mmc$ space group, where Fe and Mn atoms randomly share the 6h sites. Furthermore, other atoms of Fe, Mn, and Sn share 2c sites. The difference between the observed and calculated XRD patterns for these alloys is also shown at the bottom of each XRD pattern displayed in Figures 3.

The average crystallite sizes, estimated from the Williamson-Hall method, are in the range of 256-62 nm, indicating that some of

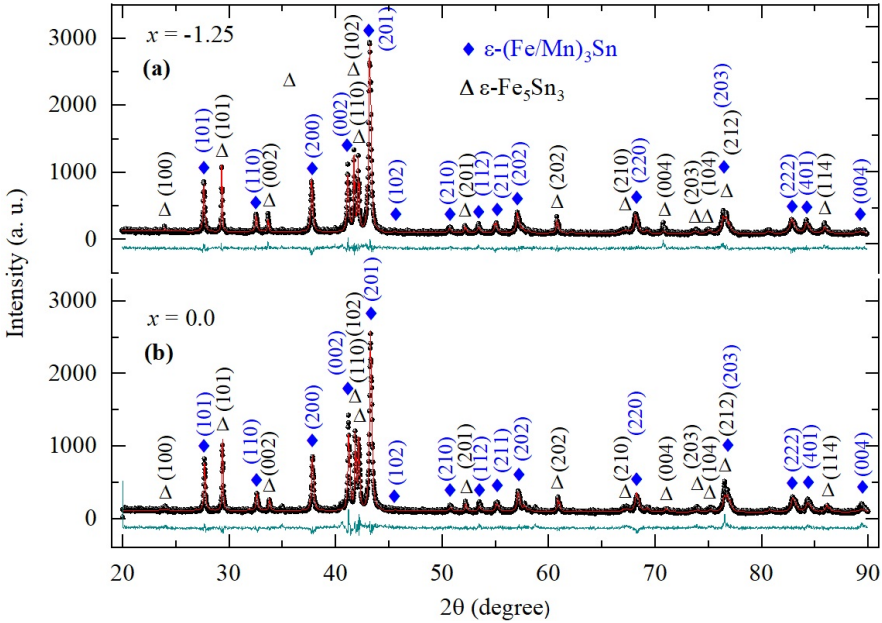


FIGURE 2. Rietveld refinement of the X-ray diffraction patterns of the annealed (a) $Fe_{50}Mn_{23.75}Sn_{26.25}$ and (b) $Fe_{50}Mn_{25}Sn_{25}$ alloys. Positions of the Bragg-reflections are shown for the (◆) $\epsilon-(Fe/Mn)_3Sn$, and (Δ) $\epsilon-Fe_5Sn_3$ phases. The difference between observed and calculated patterns and the calculated reflection positions (green color on bottom trace) is also displayed.

our samples are in the nanoscale regime (< 100 nm), while others are in micrometer size regime (bulk-like phase). A reduction in average sizes was observed as the Mn concentration increases due to a reduction in the number of nuclei during fast cooling process (see Table 1).

2.2. ^{57}Fe Mössbauer study and magnetic hyperfine properties

RT ^{57}Fe Mössbauer spectra of the annealed $Fe_{50}Mn_{23.75}Sn_{26.25}$, $Fe_{50}Mn_{25}Sn_{25}$, $Fe_{50}Mn_{27.5}Sn_{22.5}$, $Fe_{50}Mn_{30}Sn_{20}$, and $Fe_{50}Mn_{32.5}Sn_{17.5}$ alloys are respectively plotted in the Figures 4 (a), (b), (c), and (d). These spectra were fitted assuming the crystalline phases obtained from the X-ray analyses.

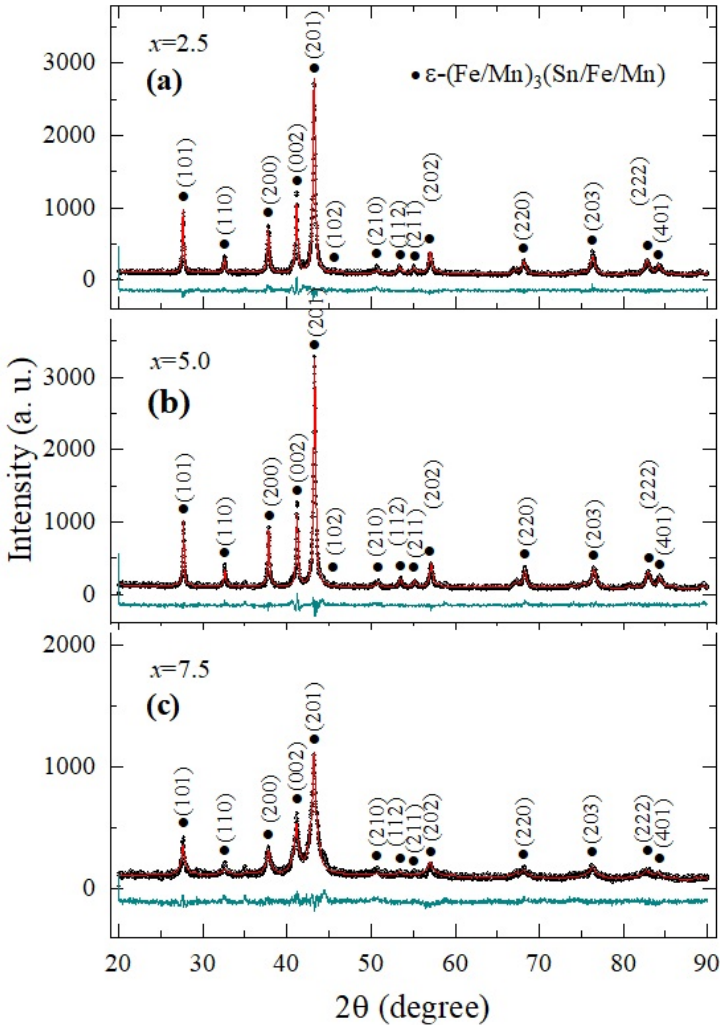


FIGURE 3. Rietveld refinement of the X-ray diffraction patterns of the annealed (a) $\text{Fe}_{50}\text{Mn}_{27.5}\text{Sn}_{22.5}$, (b) $\text{Fe}_{50}\text{Mn}_{30}\text{Sn}_{20}$, and (c) $\text{Fe}_{50}\text{Mn}_{32.5}\text{Sn}_{17.5}$. Positions of the Bragg-reflections are shown for the (\bullet) $\epsilon-(\text{Fe/Mn})_3(\text{Sn/Fe/Mn})$ phase. The difference between observed and calculated patterns and the calculated reflection positions (green color on bottom trace) is also displayed.

The ^{57}Fe Mössbauer spectra, in general, display broad six-line patterns due to nuclear Zeeman interaction [an interaction between nuclear magnetic moment and magnetic hyperfine field (B_{hf}) at Fe nucleus produced

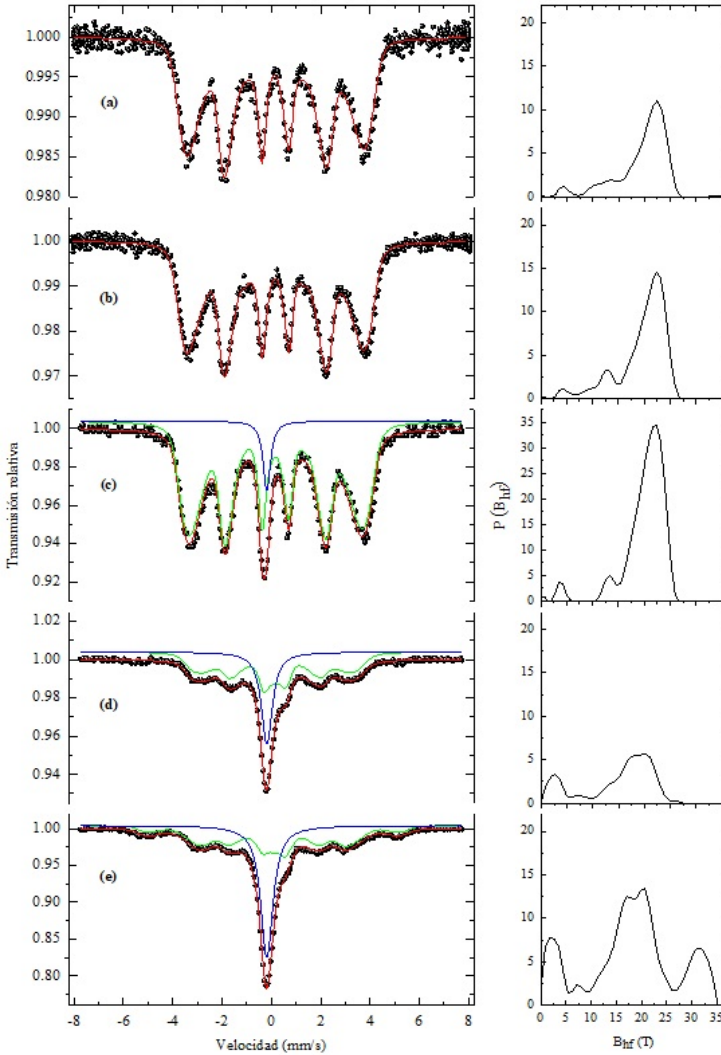


FIGURE 4. RT ^{57}Fe Mössbauer spectra of the annealed $\text{Fe}_{50}\text{Mn}_{25+x}\text{Sn}_{25-x}$ alloys with: (a) $x = -1.25$, (b) $x = 0$, (c) $x = 2.5$, (d) $x = 5$, (e) $x = 7.5$. Magnetic hyperfine field distribution $P(B_{\text{hf}})$ curves, obtained from the fits of the corresponding Mössbauer spectra, are plotted on the right-hand side for each one.

by s polarized electrons and $3d$ unpaired electrons]. The broadening line shapes of the ^{57}Fe Mössbauer spectra indicate that the Fe atoms are magnetically ordered, but there is a

distribution of Fe non-equivalent sites. This sub-spectra were fitted using a distribution of 40 magnetic hyperfine fields $P(B_{\text{hf}})$. To account for small asymmetries of the spectra, a linear correlation between B_{hf} and the isomer shift (δ) was assumed for the 40 magnetic sub-spectra.

The ^{57}Fe Mössbauer spectra of the annealed $\text{Fe}_{50}\text{Mn}_{23.75}\text{Sn}_{26.25}$ and $\text{Fe}_{50}\text{Mn}_{25}\text{Sn}_{25}$ alloys in Figures 4 (a) and (b) were fitted using a distribution of magnetic hyperfine magnetic fields $P(B_{\text{hf}})$ with 40 sub-spectra, which was associated to phase $\varepsilon-(\text{Fe}/\text{Mn})_3\text{Sn}$. The fractions of the crystalline sites of the Fe_5Sn_3 phase at 20.0 T, 20.8 T, and 24 T are less than 7 %.

The ^{57}Fe Mössbauer spectra of the annealed $\text{Fe}_{50}\text{Mn}_{27.5}\text{Sn}_{22.5}$, $\text{Fe}_{50}\text{Mn}_{30}\text{Sn}_{20}$, and $\text{Fe}_{50}\text{Mn}_{32.5}\text{Sn}_{17.5}$ alloys were also fitted using a magnetic hyperfine distribution $P(B_{\text{hf}})$ associated with the Fe magnetic sites in the $\varepsilon-(\text{Fe}/\text{Mn})_3(\text{Sn}/\text{Fe}/\text{Mn})$ hexagonal phase and a broad singlet. Indeed, the singlet must be associated with those Fe atoms in a paramagnetic state, which share the $2c$ sites with the Sn and Mn atoms. The fraction of the singlet component increases as the x-content rises. Table 2 shows the average values of the magnetic hyperfine field (B_{hf} and $B_{\text{hf}}^{\text{tr}}$) and the isomer shift (δ^{Fe} and δ^{Sn}) of non-equivalent Fe and Sn sites.

| X | $\langle B_{\text{hf}} \rangle$ (T) | $\langle B_{\text{hf}}^{\text{transf}} \rangle$ (T) | $\langle \delta^{\text{Fe}} \rangle$ (mm/s) | $\langle \delta^{\text{Sn}} \rangle$ (mm/s) | M_s (emu/g) | H_c (Oe) | M_r (emu/g) | H_{EB} (Oe) |
|-------|--|--|--|--|---------------|------------|---------------|---------------|
| -1.25 | 19.6(2) | 9.7(1) | 0.26(1) | 1.77(3) | 204.27 | 9.8(4) | 2.68(2) | 12.9(3) |
| 0.0 | 19.5(2) | 9.6(2) | 0.27(1) | 1.77(3) | 181.28 | 8.0(4) | 1.93(2) | 12.5(3) |
| 2.5 | 19.9(2) | 9.8(1) | 0.27(1) | 1.71(3) | 177.16 | 13.8(3) | 2.97(3) | 10.5(2) |
| 5.0 | 14.7(2) | 9.9(1) | 0.243(5) | 1.71(1) | 173.04 | 20.8(5) | 4.01(2) | 7.9(3) |
| 7.5 | 17.7(2) | 7.9(1) | 0.230(5) | 1.72(4) | 106.92 | 50.4(2) | 7.14(3) | 24.1(2) |

TABLE 2. Summary of magnetic parameters determined at RT for the annealed $\text{Fe}_{50}\text{Mn}_{25+x}\text{Sn}_{25-x}$ con: (a) $x = -1.25$, (b) $x = 0$, (c) $x = 2;5$, (d) $x = 5$, (e) $x = 7.5$ (magnetic hyperfine field (B_{hf}), maximum magnetization (M_s), coercive field (H_c), remnant magnetization (M_r) and exchange bias field (H_{EB})). δ^{Fe} and δ^{Sn} are the isomer shift values in Fe-site and Sn-site for each alloys.

2.3. Mössbauer study of the transferred magnetic fields in ^{119}Sn sites

Figures 5 (a), (b), (c), (d), and (e) display the RT ^{119}Sn Mössbauer spectra for the annealed $\text{Fe}_{50}\text{Mn}_{23.75}\text{Sn}_{26.25}$, $\text{Fe}_{50}\text{Mn}_{25}\text{Sn}_{25}$, $\text{Fe}_{50}\text{Mn}_{27.5}\text{Sn}_{22.5}$, $\text{Fe}_{50}\text{Mn}_{30}\text{Sn}_{20}$, and $\text{Fe}_{50}\text{Mn}_{32.5}\text{Sn}_{17.5}$ alloys, respectively. These ^{119}Sn Mössbauer spectra also show a distribution of magnetic hyperfine fields with absorption peaks between -10 mm/s and +12 mm/s. So, it clearly indicates the presence of transferred hyperfine magnetic fields ($B_{\text{hf}}^{\text{tr}}$) at the Sn sites from the conduction electron polarization effect caused by Fe and Mn atoms nearby.

The spectra were also fitted with a distribution of magnetic hyperfine fields, but now due to the transferred magnetic fields at Sn sites. A magnetic ordering of the Fe and Mn magnetic moments was assumed and then via RKKY interactions, the *s*-type conduction electrons were polarized and have lead the information to the Sn sites.

In Figures 5 (a) and (b), the ^{119}Sn Mössbauer spectra of the annealed $\text{Fe}_{50}\text{Mn}_{23.75}\text{Sn}_{26.25}$ and $\text{Fe}_{50}\text{Mn}_{25}\text{Sn}_{25}$ alloys were respectively fitted using a $P(B_{\text{hf}}^{\text{tr}})$ distribution with 40 magnetic sub-spectra. Each sub-spectrum corresponds to the transferred magnetic fields $B_{\text{hf}}^{\text{tr}}$ at Sn sites due mainly to the magnetic moments of the neighboring Fe and Mn atoms of phase $\varepsilon-(\text{Fe}/\text{Mn})_3\text{Sn}$. The ^{119}Sn Mössbauer spectra of the annealed $\text{Fe}_{50}\text{Mn}_{27.5}\text{Sn}_{22.5}$, $\text{Fe}_{50}\text{Mn}_{30}\text{Sn}_{20}$, and $\text{Fe}_{50}\text{Mn}_{32.5}\text{Sn}_{17.5}$ alloys are shown in Figures 5 (c), (d), and (e). These spectra were analyzed using a $P(B_{\text{hf}})$ distribution of 40 magnetic sub-spectra associated with $B_{\text{hf}}^{\text{tr}}$ fields at Sn sites due to *s*-type electrons polarized by Fe and Mn atoms in the hexagonal phase $\varepsilon-(\text{Fe}/\text{Mn})_3(\text{Sn}/\text{Fe}/\text{Mn})$. In addition, in the central part of the spectra corresponding to the samples with $x = 5.0$ and 7.5 , it is possible to observe a new contribution at a velocity of 1.8 mm/s (see arrows in Figures 5(d) and (e)), indicating that a small fraction of Sn atoms fees zero $B_{\text{hf}}^{\text{tr}}$ value. Thus, it can be noticed that there are regions with only Sn atoms or regions where the transferred fields of Fe and Mn are compensated (a singlet was also observed in ^{57}Fe sites).

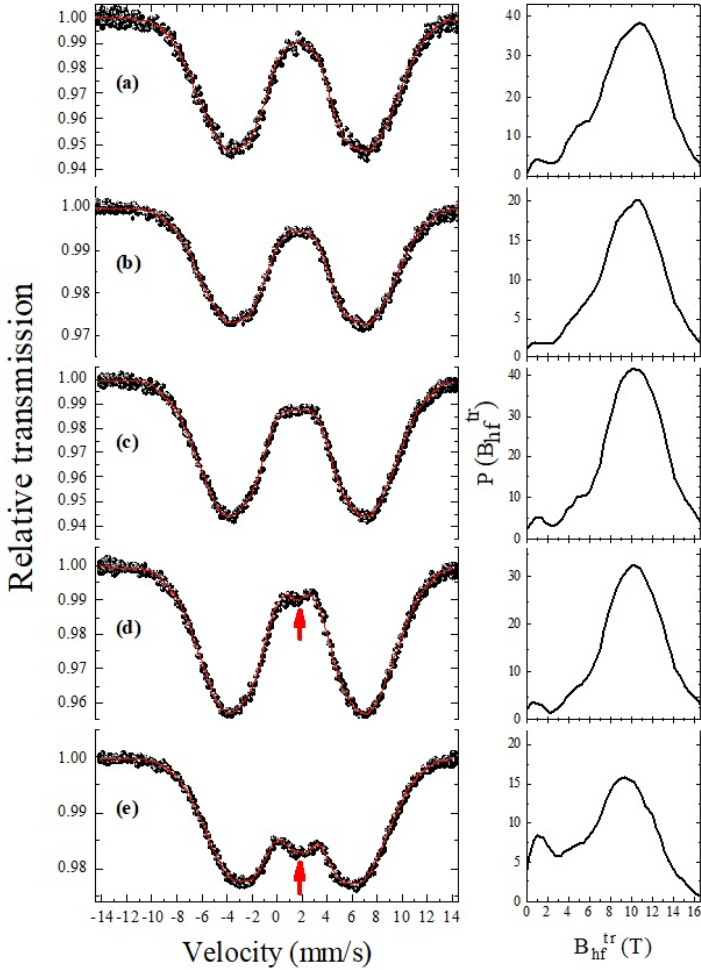


FIGURE 5. RT ^{119}Sn Mössbauer spectra of the annealed $\text{Fe}_{50}\text{Mn}_{25+x}\text{Sn}_{25-x}$ with: (a) $x = -1.25$, (b) $x = 0$, (c) $x = 2.5$, (d) $x = 5$, (e) $x = 7.5$. Magnetic hyperfine field distribution $P(B_{\text{hf}}^{\text{tr}})$ curves, obtained from the fits of the corresponding Mössbauer spectra, are plotted on the right-hand side for each one. The $B_{\text{hf}}^{\text{tr}}$ is the transferred hyperfine magnetic fields from polarized conduction s -electrons by Fe and Mn atoms. The red arrows indicate the position of paramagnetic Sn component.

2.4. RT magnetization measurements

Figure 6 shows the $M(H)$ loops of the annealed $\text{Fe}_{50}\text{Mn}_{25+x}\text{Sn}_{25-x}$ alloys. The inset presents an amplification of the central part

where a horizontal shift of the hysteresis curves relative to the zero-field was observed. The observed $M(H)$ loop shift effect (not fully understood yet in our samples) may be associated with the exchange bias effect due to the incipient formation of an antiferromagnetic phase, that arises as the Mn-Mn distances changes and by Mn excess [20]. Table 2 shows a comparison of the magnetic parameters of each alloy obtained from magnetization measurements and from ^{57}Fe and ^{119}Sn Mössbauer spectroscopies.

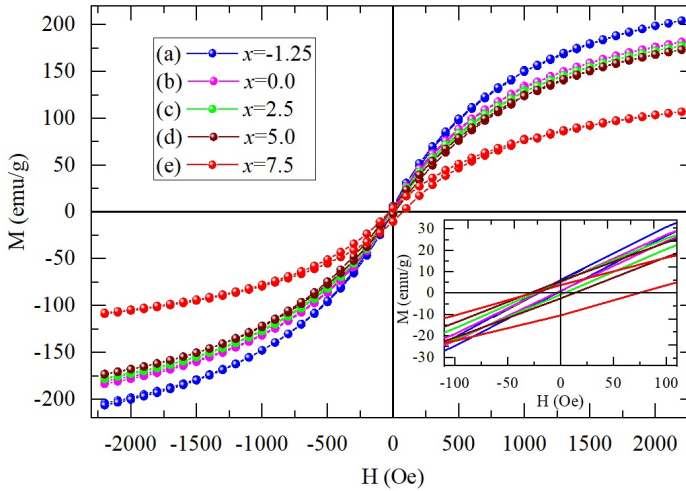


FIGURE 6. *Hysteresis curves of magnetization (M) vs. applied field (H) recorded at RT of the annealed $\text{Fe}_{50}\text{Mn}_{25+x}\text{Sn}_{25-x}$ alloys with: (a) $x = -1.25$, (b) $x = 0$, (c) $x = 2.5$, (d) $x = 5$, (e) $x = 7.5$. The inset shows the central area of the hysteresis curves of all alloys in order to highlight the horizontal shift of the curves and also the remnant and coercive fields.*

It is observed that all annealed alloys exhibit a soft ferromagnetic behavior, characterized by low values of the coercive (9.8-50.4 Oe) and remnant fields (2-7 emu/g). On the one hand, the maximum magnetization M_s (obtained with 2.2 kOe field) gradually decreases from 204.3 to 106.9 emu/g as the x-fraction of Mn increases. On the other hand, the coercive field H_c increases with the value of x, showing that the magnetic properties depend on the substitution process of Sn atoms by Mn. The highest increase of the coercive field values in the alloys with $x = 5.0$ and 7.5 is associated with the microstructural deformation and defect generation by

reduction of crystallite sizes, as shown in the XRD data. In a first approximation, there is a relationship between hyperfine magnetic field B_{hf} and Fe magnetic moments, which allows establishing some comparisons with magnetization measurements. From this comparison, it is observed that the results of the magnetization measurements are in agreement with the results from the ^{57}Fe Mössbauer spectroscopy that show a gradual increase of the singlet fraction as the x-content is increased (indirectly the Sn paramagnetic component also increases). In other words, it is also possible to establish that the observed singlets in the ^{119}Sn and ^{57}Fe Mössbauer spectra of the annealed samples with $x = 2.5, 5.0, 7.5$ are responsible for diminishing the saturation magnetization M_s when x-fraction increases.

Conclusions

Combining results of X-ray diffraction, ^{119}Sn and ^{57}Fe Mössbauer spectroscopies, and magnetization, it has been determined the structural and magnetic properties of the arc-melted and annealed $\text{Fe}_{50}\text{Mn}_{25+x}\text{Sn}_{25-x}$ Heusler alloys with $x = -1.25, 0.0, 2.5, 5.0, 7.5$. These compositions are close to those of full-Heusler Fe_2MnSn alloy, but the $L2_1$ -like cubic structure (the fingerprint of the full-Heusler) was not stabilized due to the fast quenching process (it is assumed that the thermal annealing at 1173 K and subsequently rapid cooling in iced water is responsible for the absence of the $L2_1$ -like cubic structure). The Rietveld refinement analyses of all diffractograms of the annealed $\text{Fe}_{50}\text{Mn}_{25+x}\text{Sn}_{25-x}$ alloys have shown the formation of hexagonal phases $D0_{19}$ (spatial group $P6_3/mmc$). For annealed samples with $x = -1.25$ and 0.0 , the XRD patterns have indicated two crystalline phases: (i) a disordered solid solution $\varepsilon-(\text{Fe}/\text{Mn})_3\text{Sn}$ (majority) and (ii) the intermetallic compound $\varepsilon-(\text{Fe})_5\text{Sn}_3$, whereas the alloys with $x = 2.5, 5.0$ and 7.5 have only one hexagonal phase, corresponding to a disordered crystalline solid solution, $\varepsilon-(\text{Fe}/\text{Mn})_3(\text{Sn}/\text{Fe}/\text{Mn})$. The average crystallite sizes (calculated from Williamson-Hall method) are within the range of 62-256 nm, showing that some of our alloys are in a nanoscale regime, while others are in a bulk-like one (micrometer

regime). The magnetic properties of these materials are typically similar to those found for soft magnets. They have shown low coercive and remnant fields. An increase in the coercive field of the annealed $\text{Fe}_{50}\text{Mn}_{25+x}\text{Sn}_{25-x}$ alloys is observed when the Mn fraction is increased in opposite to the behavior found for the maximum magnetization recorded at 2200 Oe. The reduction of the maximum magnetization (recorded at 2200 Oe) by increasing the atomic fraction of Mn is accompanied by the increase in the non-magnetic fraction of the ^{57}Fe and ^{119}Sn Mössbauer spectra, more pronounced in ^{57}Fe sites.

Furthermore, the Mössbauer results of the ^{57}Fe and ^{119}Sn isotopes of all annealed alloys have shown the following characteristics: (i) localized magnetism in chemically disordered systems from distribution of magnetic hyperfine fields at the Fe sites, and (ii) of itinerant magnetism originated by transferred hyperfine fields from the neighboring Fe and Mn atoms in the ^{119}Sn nuclei. Alloys with $x = 2.5, 5.0,$ and 7.5 have also shown a small non-magnetic fraction due to regions with a higher concentration of Sn or regions where the transferred field of the Fe and Mn atoms is canceled.

Acknowledgments

The authors would like to acknowledge the financial support provided by local organizations through the projects: 121301201 (Major National University of San Marcos, UNMSM) and contract 011-2014-FONDECYT (National Fund for Scientific and Technological Development, FONDECYT), and for the support of international cooperation organizations, FAPERJ-Brazil, FINEP, FAPES, CNPq and the Latin American Center for Physics.

References

- [1] T. Krenke, M. Acet, E. F. Wassermann, X. Moya, L. Mañosa, and A. Planes, *Phys. Rev. B* **72**, 014412 (2005).
- [2] T. Krenke, E. Duman, M. Acet, E. F. Wassermann, X. Moya, L. Mañosa, and A. Planes, *Nature Mater.* **4**, 450 (2005).

- [3] K. Koyama, T. Kanomata, R. Kainuma, K. Oikawa, K. Ishida, and K. Watanabe, *Physica B* **383**, 24 (2006).
- [4] P. J. Brown, A. P. Gandy, K. Ishida, R. Kainuma, T. Kanomata, K.-U. Neumann, K. Oikawa, B. Ouladdiaf, and K. R. A. Ziebeck, *J. Phys.: Condens. Matter* **18**, 2249 (2006).
- [5] R. Kainuma, Y. Imano, W. Ito, H. Morito, Y. Sutou, K. Oikawa, A. Fujita, K. Ishida, S. Okamoto, O. Kitakami, and T. Kanomata, *Appl. Phys. Lett.* **88**, 192513 (2006).
- [6] S. Aksoy, T. Krenke, M. Acet, E. F. Wassermann, X. Moya, L. Mañosa, and A. Planes, *Appl. Phys. Lett.* **91**, 251915 (2007).
- [7] T. Krenke, E. Duman, M. Acet, X. Moya, L. Mañosa, and A. Planes, *J. Appl. Phys.* **102**, 033903 (2007).
- [8] I. Galanakis, E. Şaşıoğlu, and K. Özdoğan, *Phys. Rev. B* **77**, 214417 (2008).
- [9] R. Kainuma, K. Oikawa, W. Ito, Y. Sutou, T. Kanomata, and K. Ishida, *J. Mater. Chem.* **18**, 1837 (2008).
- [10] E. Şaşıoğlu, L. M. Sandratskii, and P. Bruno, *Phys. Rev. B* **77**, 064417 (2008).
- [11] A. L. Alves, E. C. Passamani, V. P. Nascimento, A. Y. Takeuchi, and C. Larica, *J. Phys. D: Appl. Phys.* **43**, 345001 (2010).
- [12] E. C. Passamani, F. Xavier, E. Favre-Nicolin, C. Larica, A. Y. Takeuchi, I. L. Castro, and J. R. Proveti, *J. Appl. Phys.* **105**, 033919 (2009).
- [13] S. Chatterjee, V. R. Singh, A. K. Deb, S. Giri, S. K. De, I. Dasgupta, and S. Majumdar, *J. Magn. Magn. Mater.* (2010).
- [14] C. Hurd and S. McAlister, *J. Magn. Magn. Mater.* **61**, 114 (1986).
- [15] E. Uhl, *J. Solid State Chem.* **43**, 354 (1982).
- [16] S. Fujii, S. Ishida, and S. Asano, *J. Phys. Soc. Jpn.* **64**, 185 (1995).
- [17] V. K. Jain, N. Lakshmi, V. Jain, S. A. K., and K. Venugopalan, *AIP Conf. Proc.* **1665**, 130032 (2015).

- [18] V. K. Jain, N. Lakshmi, and R. Jain, *AIP Conf. Proc.* **1953**, 110007 (2018).
- [19] V. K. Jain, N. Lakshmi, R. Jain, and A. R. Chandra, *J. Supercond. Nov. Magn.* **32**, 739 (2019).
- [20] E. C. Passamani, F. Xavier, E. Favre-Nicolin, C. Larica, A. Y. Takeuchi, I. L. Castro, and J. R. Proveti, *J. Appl. Phys.* **105**, 033919 (2009).